Model Study of the Q-factor of a Varicap Diode by Its Equivalent Circuits

Andrii V. Rudyk[a], Andriy O. Semenov[b], Olena O. Semenova[b], Serhii M. Tsyrulnyk[c] and Volodymyr D. Tromsyuk[d]

[a] *National University of Water and Environmental Engineering, Soborna street, 11, 33000, Rivne, Ukraine*
[b] *Vinnytsia National Technical University, Khmelnytske highway, 95, Vinnytsia, 21021, Ukraine*
[c] *Vinnytsia National Agrarian University, str. Sonyachna, 3, City, Vinnytsia, 21008, Ukraine*
[d] *Vinnytsia Technical College, Khmelnytske highway, 91/2, Vinnytsia, 21021, Ukraine*

Abstract

In this study, the authors showed that the Q-factor of a varicap diode depends on frequency and is a function of parameters of its small-signal equivalent circuit. Influence of the equivalent circuit parameters on the varicap diode Q-factor in ranges of low and high frequencies was analyzed. Equations for determining the maximum value of the varicap diode Q-factor and a frequency that corresponds to the extreme value of the Q-factor were obtained. Theoretical results were experimentally verified for three different varicap diodes of BB1xx types manufactured by NXP Semiconductors. Deviations of theoretical results from experimental testing in the (20–500) MHz frequency range do not exceed 8.6%. For varicap diodes of BB149 and BB174 types, the frequency ranges were established, in which their Q-factor was more than 35; and for a varicap diode of BB181 type the frequency ranges were established, in which its Q-factor was more than 15. Parameters of elements of series and parallel equivalent circuits of the varicap diode were determined. Frequency dependences of active and reactive components of the series and parallel equivalent circuits of the varicap diode were analyzed. For three types of varicap diodes, frequency ranges were determined in which difference between an equivalent capacitance of the equivalent circuit and a barrier capacitance was less than 0.5%, and difference between an equivalent resistance of the equivalent circuit and a loss resistance in the emitter and base regions was less than 3%. It was proved that in the frequency range where the varicap diode Q-factor was greater than 35 (BB149 and BB174) or 15 (BB181), the equivalent capacitances of series and parallel equivalent circuits can be regarded as independent of frequency and equal to the capacitance of the varicap diode junction with an error of less than 0.5%.

Keywords 1

Varicap diode, Q-factor, model study, mathematical model, equivalent circuit

1. Introduction

Varicap diodes are used as electrically controlled capacitances in oscillatory circuits of telecommunication and information-measuring systems for various purposes. The operating principle of a varicap diode is based on dependence of the barrier capacitance of an electrical junction on the applied reverse voltage [1, 2]. This dependence is the capacitance-voltage characteristic of the varicap diode.

ITTAP'2022: 2nd International Workshop on Information Technologies: Theoretical and Applied Problems, November 22–24, 2022, Ternopil, Ukraine
EMAIL: a.v.rudyk@nuwm.edu.ua (A. Rudyk); semenov.a.o@vntu.edu.ua (A. Semenov); semenova.o.o@vntu.edu.ua (O. Semenova); sovmsvom@gmail.com (S. Tsyrulnyk); 2013tvd@gmail.com (V. Tromsyuk)
ORCID: 0000-0002-5981-3124 (A. Rudyk); 0000-0001-9580-6602 (A. Semenov); 0000-0001-5312-9148 (O. Semenova); 0000-0002-5703-9761 (S. Tsyrulnyk); 0000-0001-5022-8159 (V. Tromsyuk)

For efficient use of the varicap diode in high-frequency circuits, a frequency range must be determined, in which its Q-factor will be maximum or exceed a given value, by equivalent parameters of its small-signal circuit. Also, to simplify analysis in an operating frequency range, the varicap diode can be represented by one of the simplified equivalent circuits proposed in this paper.

Varicap diodes are being utilized in phase locked loops [3, 4]. Moreover, they are being utilized and in such devices as voltage-controlled oscillators [5, 6], frequency modulators [7, 8], comparators [9, 10], variable phase shifters [11, 12], bandpass filters [13, 14], power amplifiers [15, 16].

A simple but effective method to reduce reference spurs in analog subsampling phase locked loops by applying a varicap diode cancellation technique is presented in [3]. A fully synthesizable injection-locking based phase locked loop with an interpolative phase-coupled oscillator, a digital-to-analog converter with current output, and a digital varicap diode with fine resolution are discussed in [4]. Here, all circuits making up the phase locked loop were designed and implemented by standard elements without any modification.

A variation-aware design methodology for a high-performance MOS-varactor voltage-controlled ring oscillator (MV-VCRO) in near-threshold-voltage (NTV) mode was proposed in [5]. Delay-models for conventional, bulk-driven, and dynamic-threshold oscillators allowing for nonlinearity in near-threshold-voltage mode are considered using MOS-varactor capacitance models and effective drive current. Effects of supply-induced frequency variations on single-ended tuning LC voltage-controlled oscillator that degrade the jitter performance of the clock are examined in [6]. Moreover, a compensation technique is proposed, which applies complementary varactors for increasing the supply sensitivity of single-ended tuning oscillator. The varactor effective capacitance changes with the supply voltage, which impacts the supply sensitivity.

A W-band vector modulator, which based on vector summing with a Gilbert cell, is discussed in [7]. Here two error-reducing schemes are applied to a summing circuit. One is to apply current sources, which consist of short channel transistors, to take advantage of the so-called channel length modulation effect. The other scheme implements impedance correction varactors at input. It controls gain and phase with a digital-to-analog converter, which makes the output impedance of the summing circuit constant. An approach to a frequency modulation by employing a split-ring resonator loaded with a varactor diode is considered in [8]. There, the modulation occurs because of a continuous variety of the varactor diode capacitance by changing its bias voltage by a signal which is to be modulated. The frequency range of modulated signals can be controlled by adjusting varactor parameters.

A differential time-domain comparator, which is formed by two voltage controlled delay lines – one per input terminal, as well as a binary phase detector for comparison solving were discussed in [9]. A set of digitally controlled inversion-mode varactors is utilized for adjusting propagation delay through respective lines. Such varactors provide tuning capabilities to the time-domain comparator; which features can be used for offset calibration. An offset calibration approach is presented in [10]. This approach uses dynamic characteristics of a comparator in order to obtain a wide linear tuning range by locating varactors at two different internal nodes – drains of the input pairs (for high linearity) and output nodes (for wider compensation range). The comparators are implemented in a 3-bit 1GS/s flash ADC, which can be integrated into an 8-bit hybrid ADC architecture.

A low loss reflection-type phase shifter is introduced in [11]. This shifter applies a varactor diode as a load. A performed analysis showed that a real part of the load affects phase variation and insertion loss. A variable phase shifter is presented in [12]. This shifter has a 360° range and may be employed in X-band phased arrays. The regarded system consists of a branchline coupler, variable reflection loads on varactor diodes, and a switched line topology. The reflective loads are quite compact and require only one control voltage for the varactor diodes, so the control circuit is very simplified.

A tunable suspended integrated stripline bandpass filter based on a varactor is developed in [13]. Surface mount varactors are implemented on the filter that provides frequency tuning by using reverse biasing of the varactors at different voltages. A microstrip balun bandpass filter having a tunable center frequency is introduced in [14]. Such structure has open loop resonators on varactor diodes, which are employed for tuning a resonant frequency.

A wideband output combiner which can be used for outphasing power amplifier is considered in [15]. Two non-commensurate transmission lines are superseded with two reconfigurable T-type networks, with shunt varactors as a load. A multiband switchable low-noise amplifier is presented in [16]. The operation bands can be tuned by using a varactor-based tunable network as an interstage

matching circuit, moreover it promotes covering the 5G frequency bands N257/N260. The developed tunable structure operates without sacrificing noise performance and requires no increase in DC consumption and in a chip size.

The purpose of this work is a model study of the frequency dependence of the varicap diode Q-factor on elements of its small-signal equivalent circuit and experimental investigation of BB1xx-type varicap diodes to confirm the adequacy of obtained theoretical results.

2. Parameters and equivalent circuits of the varicap diode

The main parameters of the varicap diodes related to the Q-factor are [17]:

- a nominal Q-factor of the varicap diode $Q_V(\omega)=\frac{X_V(\omega)}{R_V(\omega)}$, it is the ratio of the varicap diode reactance $X_V(\omega)$ to the total loss resistance $R_V(\omega)$ at a nominal bias voltage U_{nom} at a given frequency;
- the temperature coefficient of Q-factor $TK\,Q_V=\frac{d\,Q_V}{Q_V\,dT}$, it is a relative change in the varicap diode Q-factor when the ambient temperature changes by 1 K in a given temperature range;
- the frequency range of the varicap diode $f_{\min}\div f_{\max}$, which is determined by limiting frequencies at which $Q_V(f_{\min})=Q_V(f_{\max})=1$;
- limiting frequencies of the varicap diode $f_{\min}=\frac{1}{2\pi C_T R_T}$ and $f_{\max}=\frac{1}{2\pi C_T r_S}$, where $r_S=r_E+r_B$ is the resistance of losses in emitter and base regions of the varicap diode; R_T is the varicap diode reverse resistance when the reverse voltage U_{rev} is applied; C_T is the junction capacitance (barrier capacitance).

Since the varicap diode is a high quality element, its Q-factor is evaluated by equivalent circuits or by different measurement methods. When the resonance method is used, the varicap diode is implemented in a measuring resonant circuit. The varicap diode Q-factor is estimated from known parameters of the resonant circuit and the measured resonant frequency and Q-factor of the circuit with the varicap diode. Therefore, in this case, it is important to accurately determine parameters of the measuring resonant circuit. When the amplitude-phase measurement method [18] is applied to evaluate the varicap diode Q-factor, the phase shift between voltages on the varicap diode and an exemplary element and the ratio of amplitudes of these voltages are measured.

The paper [1] presents a general nonlinear model of a p-n junction (varicap diode) for a large signal mode, that is, when currents and voltages change within arbitrary limits. The main elements of such model are a loss resistance r_S, a reverse junction resistance R_T, which allows for a thermal generation current in the junction and a leakage current, and a barrier capacitance C_T. In general, the reverse junction resistance R_T is a function of a reverse voltage U_{rev}. For practical equivalent circuits, R_T is a fixed resistor corresponding to a linear approximation of the reverse branch of the static characteristic in a given range of change in U_{rev}. Its resistance has a value of tens of kΩ, therefore, with a forward bias, it practically does not affect the current.

The model presented in [19] differs from the previous one by the presence of a capacitor C_B to allow for parasitic capacitances of the leads and the varicap diode case, a resistor r_d to take into account the differential resistance of the junction and an inductance L_p of the varicap diode leads.

The most common equivalent small-signal varicap diode circuit (Figure 1,a) [17] consists of lead inductances $L_p \le 3\,nH$, package capacitance $C_B \le 1.5\,pF$ [19], loss resistance r_S, reverse p-n junction resistance R_T, differential p-n junction resistance r_d, and barrier capacitance C_T.

Such a varicap diode model is simplified, since it does not allow for the effect of the loss resistance modulation in the base region, the recombination current, the breakdown, the frequency dependence of the barrier capacitance, and other phenomena. To consider such effects, additional components must be introduced into the varicap diode equivalent circuit. However, complication of the equivalent circuit when additional components are included in it leads to a complication of its analysis and does not always increase the reliability of obtained results.

3. Model study of the Q-factor of the varicap diode by its equivalent circuits

The total resistance of the varicap diode by the equivalent small-signal circuit (Figure 1,a) is:

$$Z_V(i\omega) = i2\omega L_p + \frac{\frac{1}{i\omega C_B}\cdot\left[r_S + \frac{\frac{R_T r_d}{R_T + r_d}\cdot\frac{1}{i\omega C_T}}{\frac{R_T r_d}{R_T + r_d} + \frac{1}{i\omega C_T}}\right]}{\frac{1}{i\omega C_B} + r_S + \frac{\frac{R_T r_d}{R_T + r_d}\cdot\frac{1}{i\omega C_T}}{\frac{R_T r_d}{R_T + r_d} + \frac{1}{i\omega C_T}}} = i2\omega L_p + \frac{r_S + \frac{R_T r_d}{R_T + r_d + i\omega C_T R_T r_d}}{1 + i\omega C_B r_S + \frac{i\omega C_B R_T r_d}{R_T + r_d + i\omega C_T R_T r_d}} = \quad (1)$$

$$= \frac{R_T^2(r_S + r_d) + r_d^2(R_T + r_S) + 2R_T r_S r_d + \omega^2 C_T^2 R_T^2 r_S r_d^2}{\left(R_T + r_d - \omega^2 C_T C_B R_T r_S r_d\right)^2 + \omega^2\left[C_B(R_T r_S + R_T r_d + r_S r_d) + C_T R_T r_d\right]^2} -$$

$$-i\frac{\omega^3\left\{C_T^2 C_B R_T^2 r_S^2 r_d^2 - 2L_p\left[C_B(R_T r_S + R_T r_d + r_S r_d) + C_T R_T r_d\right]^2\right\} + \rightarrow}{\left(R_T + r_d - \omega^2 C_T C_B R_T r_S r_d\right)^2 + \rightarrow} \rightarrow$$

$$\rightarrow \frac{\rightarrow + \omega\left\{C_B\left[2R_T r_S r_d(R_T + r_S + r_d) + R_T^2(r_S^2 + r_d^2) + r_S^2 r_d^2\right] + C_T R_T^2 r_d^2 - 2L_p\left(R_T + r_d - \omega^2 C_T C_B R_T r_S r_d\right)^2\right\}}{\rightarrow + \omega^2\left[C_B(R_T r_S + R_T r_d + r_S r_d) + C_T R_T r_d\right]^2} =$$

$$= \mathrm{Re}_V(\omega) - i\,\mathrm{Im}_V(\omega) = R_V(\omega) - i\,X_V(\omega).$$

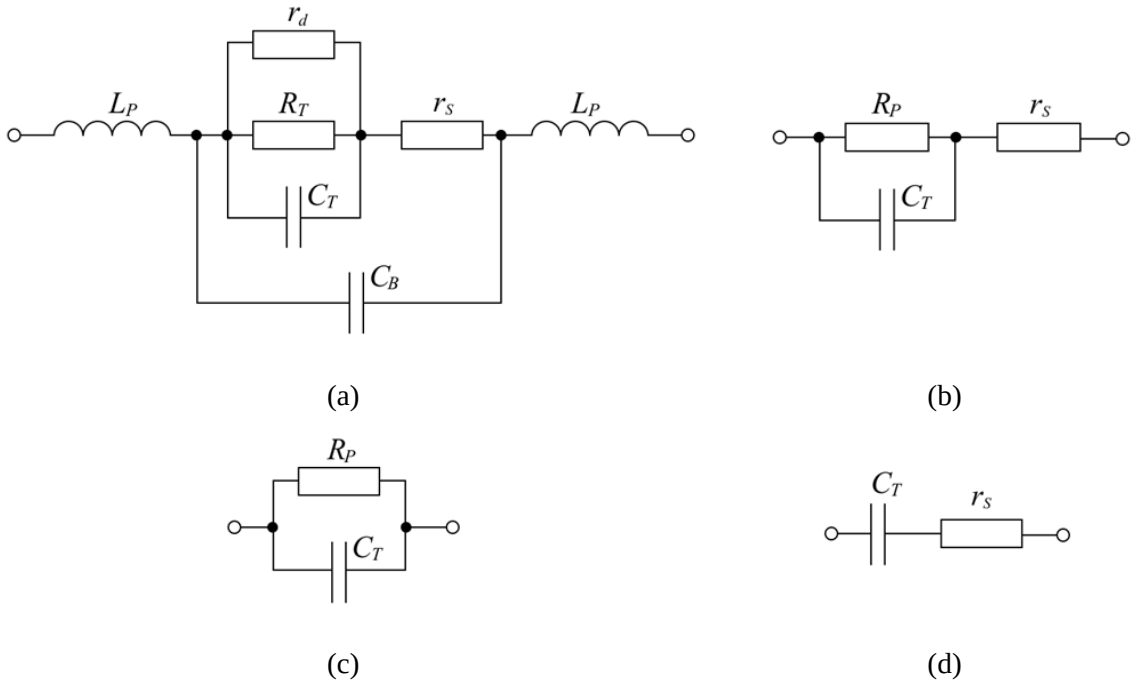

Figure 1: Varicap diode equivalent circuits: (a) Complete circuit for small signal; (b) Simplified; (c) Low-frequency simplified; (d) High-frequency simplified

The varicap diode Q-factor by its total small-signal equivalent circuit (Figure 1,a) is:

$$Q_V(\omega)=\frac{\mathrm{Im}_V(\omega)}{\mathrm{Re}_V(\omega)}=\frac{X_V(\omega)}{R_V(\omega)}=\frac{\omega^3\left\{C_T^2C_BR_T^2r_S^2r_d^2-2L_p\left[C_B\left(R_Tr_S+R_Tr_d+r_Sr_d\right)+C_TR_Tr_d\right]^2\right\}+\rightarrow}{R_T^2\left(r_S+r_d\right)+r_d^2\left(R_T+r_S\right)+2R_Tr_Sr_d+\rightarrow}\rightarrow \quad (2)$$

$$\rightarrow\frac{\rightarrow+\omega\left\{C_B\left[2R_Tr_Sr_d\left(R_T+r_S+r_d\right)+R_T^2\left(r_S^2+r_d^2\right)+r_S^2r_d^2\right]+C_TR_T^2r_d^2-2L_p\left(R_T+r_d-\omega^2C_TC_BR_Tr_Sr_d\right)^2\right\}}{\rightarrow+\omega^2C_T^2R_T^2r_S^2r_d^2}.$$

The authors examined frequency dependencies for the Q-factor of varicap diodes of BB149, BB174 and BB181 types produced by NXP Semiconductors. Table 1 presents SPICE Model parameters for these varicap diodes [20-22].

Table 1

SPICE Model Parameters of varicap diodes

Type	C_T	U_{rev}	r_s	R_T	r_d	R_P	C_B	L_P
	(pF)	**(V)**	**(Ω)**	**(kΩ)**	**(kΩ)**	**(kΩ)**	**(pF)**	**(nH)**
BB149	1.9-19.5	0.5-28	0.75	85	7.33	6.75	0.22	0.85
BB174	1.95-21.26	0.5-28	0.6	78	6.75	6.21	0.15	0.65
BB181	0.7-17.0	0.5-28	3.0	125	7.5	7.08	0.35	1.25

Allowing for formula (2), the authors constructed graphs of $Q_V=f\left(C_T,f\right)$ (Figure 2) at the change in junction capacitance in the (2-20) pF range for varicap diodes of BB149 and BB174 types and in the (1-17) pF range for the varicap diode of BB181 type, with frequency changing in the range (20-500) MHz.

The Q-factor lies in the (15-25) range for different types of varicap diodes at frequencies of the (20~50) MHz order and at a minimum reverse voltage of (0.5-1) V. The value of the varicap diode Q-factor decreases with increasing reverse voltage (with decreasing barrier capacitance). As the frequency increases, the varicap diode Q-factor increases and reaches its extremum. With a further increase in the frequency for the varicap diode equivalent circuit (Figure 1,a) we obtain a negative Q-factor at frequencies above 700 MHz. This can be explained by the fact that at high frequencies the varicap diode reactance of becomes inductive, since the inductive resistance of the varicap diode leads becomes greater than the junction capacitance (Figure 3).

Formula (2) is difficult for practical evaluation of the varicap diode Q-factor. Therefore, at frequencies up to several hundreds of MHz, one can neglect parameters L_p and C_B of the equivalent small-signal circuit, denote $R_P=\frac{R_Tr_d}{R_T+r_d}$, and limit to a simplified equivalent circuit (Figure 1,b). In this case, the typical value of reverse resistance of the varicap diode junction is $R_T>50\,k\Omega$ [23].

The total resistance of the varicap diode according to the simplified equivalent circuit (Figure 1,b) is:

$$Z_V(i\omega)=r_S+\frac{R_P\cdot\frac{1}{i\omega C_T}}{R_P+\frac{1}{i\omega C_T}}=\frac{R_P+r_S+\omega^2C_T^2R_P^2r_S-i\omega C_TR_P^2}{1+\omega^2C_T^2R_P^2}= \quad (3)$$

$$=\frac{R_P+r_S+\omega^2C_T^2R_P^2r_S}{1+\omega^2C_T^2R_P^2}-i\frac{\omega C_TR_P^2}{1+\omega^2C_T^2R_P^2}=\mathrm{Re}_{V1}(\omega)-i\,\mathrm{Im}_{V1}(\omega)=R_{V1}(\omega)-i\,X_{V1}(\omega).$$

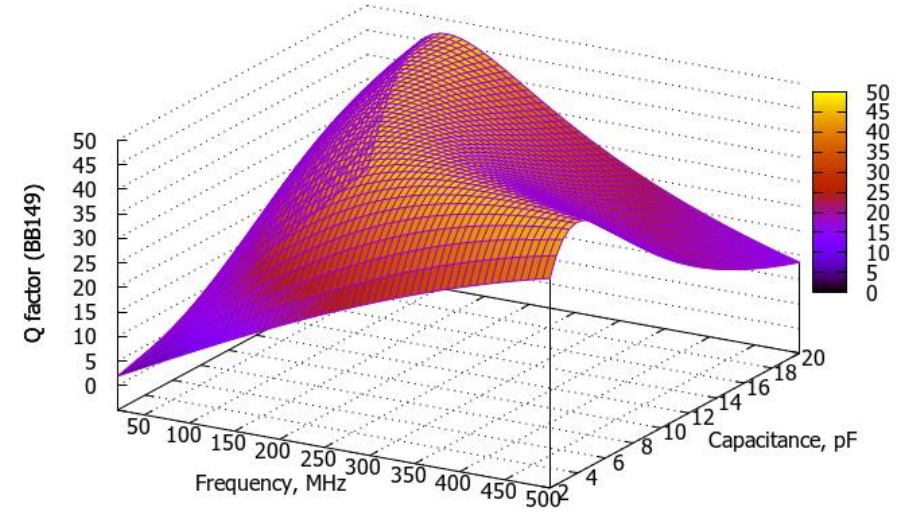

(a)

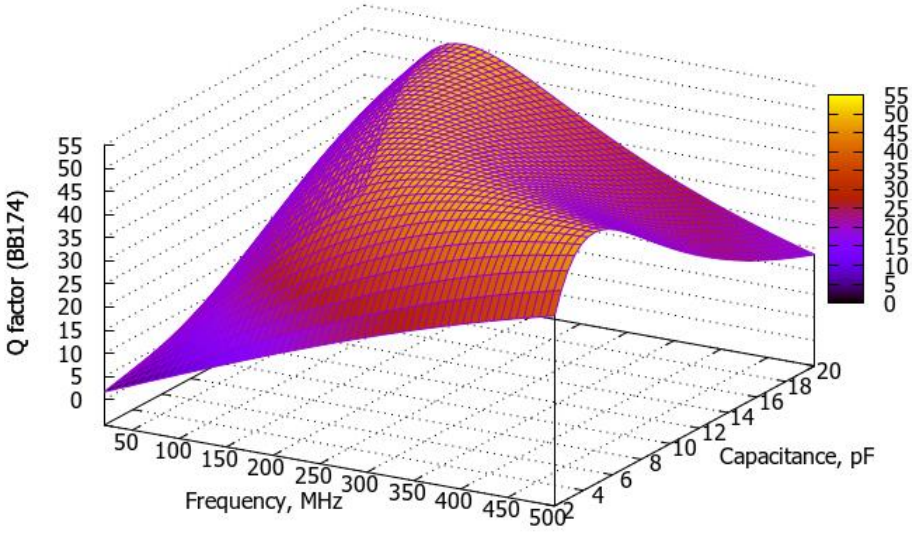

(b)

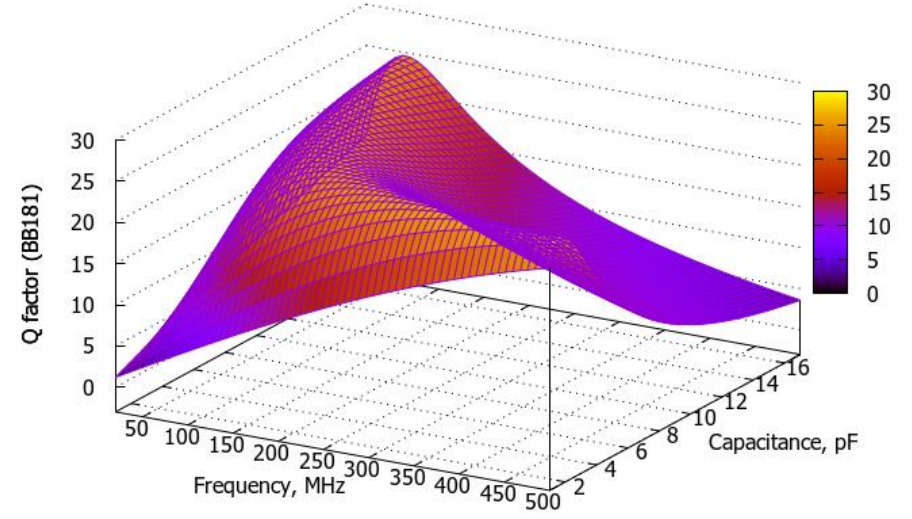

(c)

Figure 2: Graphs of dependencies $Q_V = f\left(C_T, f\right)$ for varicap diodes of BB149(a), BB174(b) and BB181(c) types

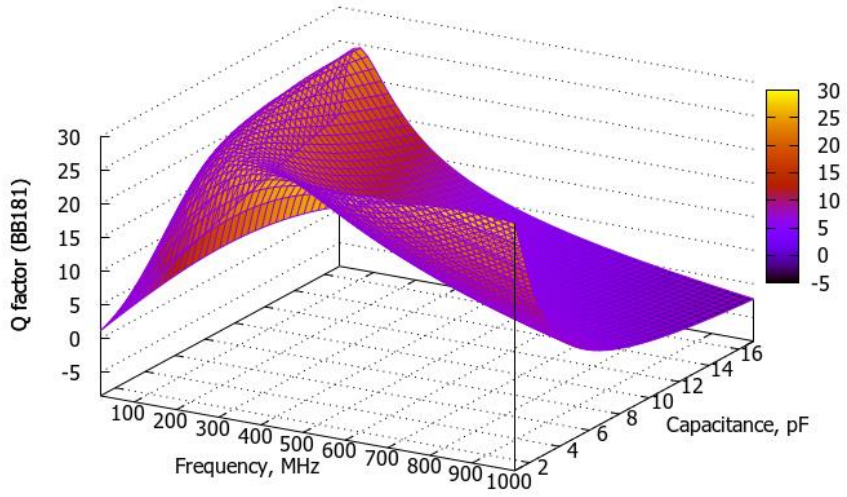

Figure 3: Dependence $Q_V = f\left(C_T, f\right)$ for the varicap diode of BB181 type in the (20-1000) MHz frequency range

The varicap diode Q-factor according to the simplified equivalent circuit (Figure 1,b) is:

$$Q_{V1}(\omega) = \frac{\mathrm{Im}_{V1}(\omega)}{\mathrm{Re}_{V1}(\omega)} = \frac{X_{V1}(\omega)}{R_{V1}(\omega)} = \frac{\omega C_T R_P^2}{R_P + r_S + \omega^2 C_T^2 R_P^2 r_S}. \quad (4)$$

According to formula (4), the resistance r_S determines the varicap diode Q-factor at high frequencies. To increase the Q-factor when an n^+-region is introduced into the varicap diode, resistance of the base must be reduced and so does resistance of the contact by choosing its material and increasing concentration of impurities in the n^+-region of the base [24].

To evaluate the reliability of the simplified equivalent circuit of the varicap diode (Figure 1,b), the authors determined dependences of relative deviation of the Q-factor estimate $s_{Q_V} = \left(1 - \frac{Q_{V1}(\omega)}{Q_V(\omega)}\right) \cdot 100\%$ for varicap diodes of BB149, BB174, and BB181 types (Figure 4) on junction capacitance and frequency considering the equivalent circuits in Figures 1,a,b (formulas (2) and (4)).

The value of the Q-factor relative deviation increases when the frequency increases and the reverse voltage decreases. The maximum deviation of the Q-factor was in varicap diodes with maximum barrier capacitance (among studied ones, this is a varicap diode of SMV2023-011LF type).

In this study the authors estimated the maximum frequency of an operating frequency range of the varicap diode equivalent circuits (Figures 1,a,b) in case when the reactance of the varicap diode was at least 10 times greater than the inductive resistance of its outputs. For the complete equivalent circuit (Figure 1,a), this condition is as follows:

$$\frac{-2\omega^5 L_P C_B^2 C_T^2 r_S^2 R_P^2 + \omega^3 \left\{ C_T^2 C_B R_P^2 r_S^2 - 2L_P \left[C_B^2 \left(R_P + r_S\right)^2 + C_T R_P^2 \left(C_T + 2C_B\right) \right] \right\} + \rightarrow}{\left(1 - \omega^2 C_T C_B R_P r_S\right)^2 + \rightarrow} \rightarrow$$

$$\rightarrow \frac{\rightarrow + \omega \left[C_B \left(R_P + r_S\right)^2 + C_T R_P^2 - 2L_P \right]}{\rightarrow + \omega^2 \left[C_B \left(R_P + r_S\right) + C_T R_P \right]^2} > 10\omega L_p. \quad (5)$$

The authors estimated graphically the maximum frequency of the operating frequency range of the varicap diodes equivalent circuits (Figures 1,a,b) under this condition as shown in Figure 5.

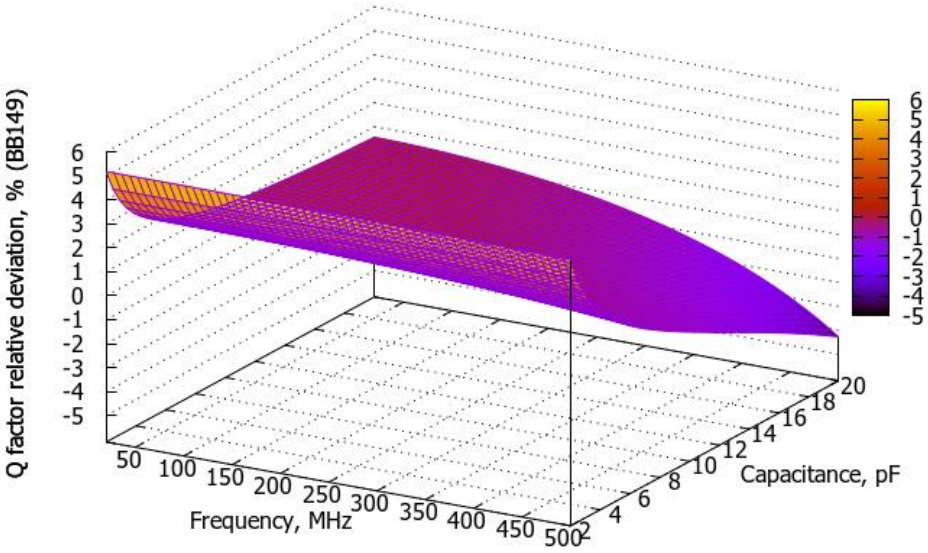

(a)

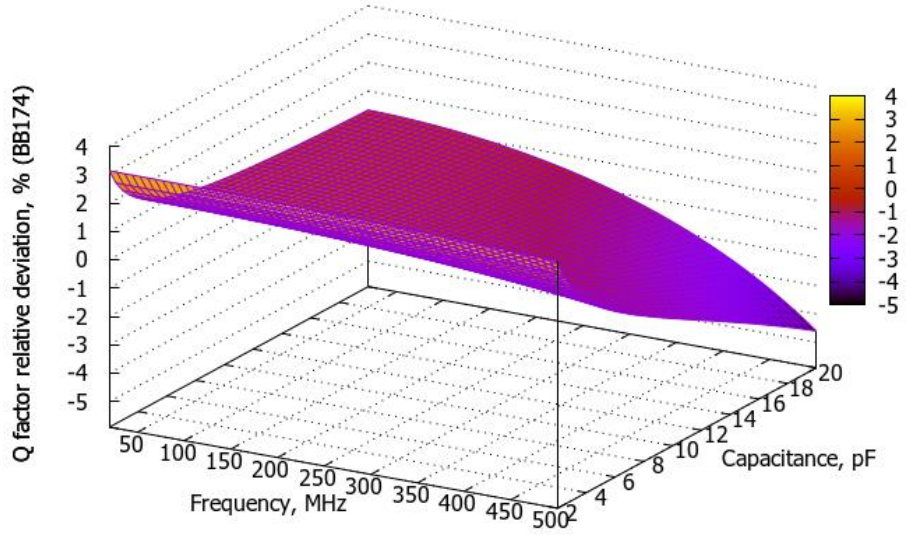

(b)

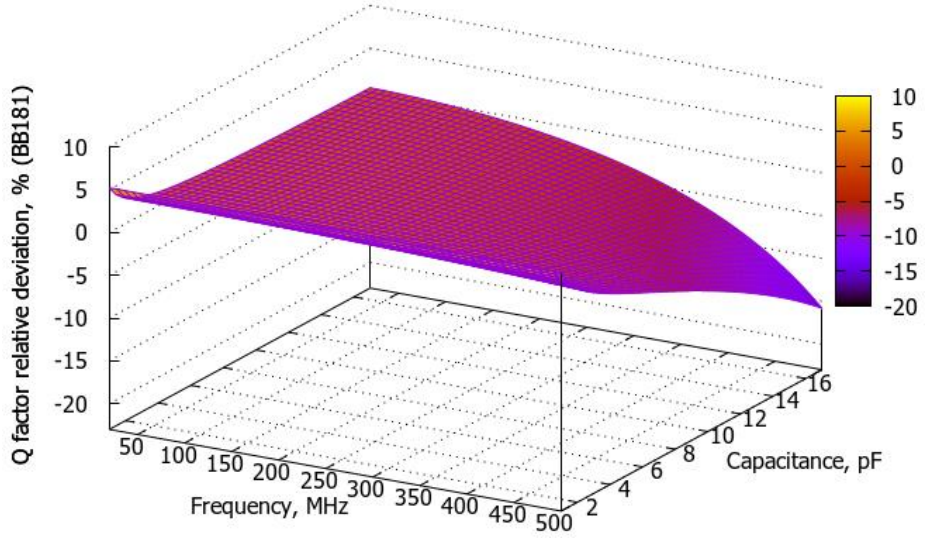

(c)

Figure 4: Dependences of relative deviation of the Q-factor $s_{Q_V} = f\left(C_T, f\right)$ for varicap diodes of BB149(a), BB174(b) and BB181(d) types

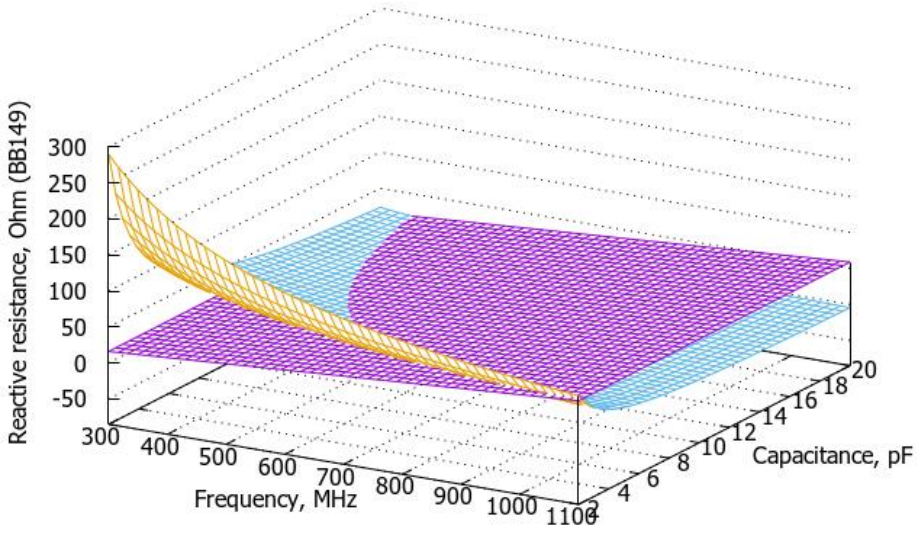

(a)

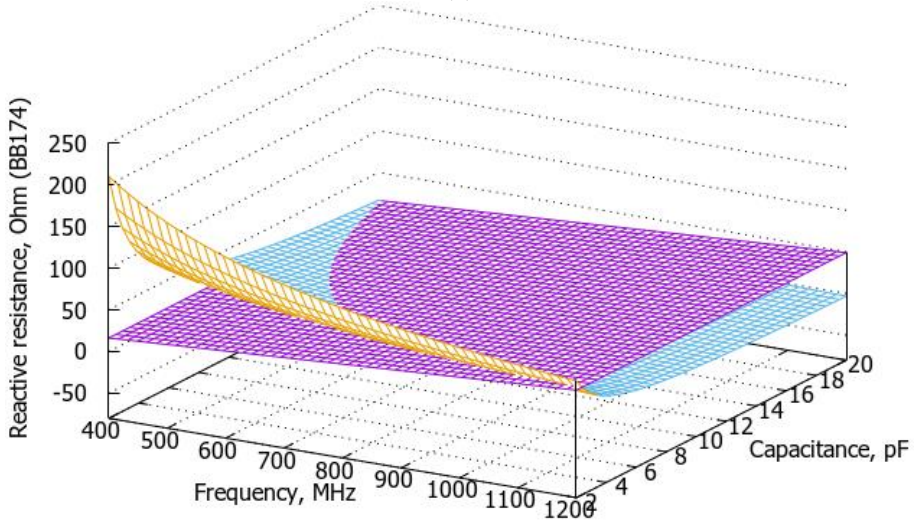

(b)

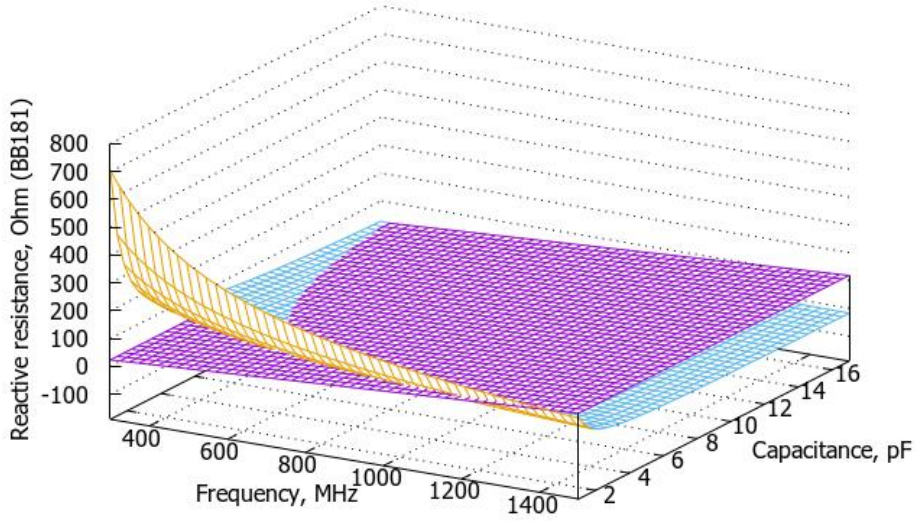

(c)

Figure 5: Dependences of varicap diode reactance $X_V = f\left(C_T, f\right)$ for estimating the maximum frequency of the operating frequency range of equivalent circuits for varicap diodes of BB149(a), BB174(b) and BB181(c) types

The operating frequency ranges for varicap diodes of the selected types are from 390 MHz at maximum capacitance of 19.5 pF to 1100 MHz at minimum capacitance of 1.95 pF for the BB149 type varicap diode, from 430 MHz at maximum capacitance of 21.26 pF to 1200 MHz at minimum capacitance of 1.95 pF for the BB174 type varicap diode, from 330 MHz at maximum capacitance of 17 pF to 1300 MHz at minimum capacitance of 0.7 pF for the BB181 type varicap diode (Figure 5). The authors concluded that the decrease in the maximum operating frequency of the varicap diode is determined by an increase in its barrier capacitance and depends on the reverse voltage U_{rev}.

At lower frequencies at $\omega C_T r_S << 1$, the varicap diode equivalent circuit is a parallel connection of R_P and C_T (Figure 1,c), its Q-factor is determined by the formula $Q_{V1.LF}(\omega) \approx \omega C_T R_P$ and it linearly depends on frequency. At high frequencies at $\omega C_T R_P >> 1$, the equivalent circuit is a series connection of r_S and C_T (Figure 1,d), the varicap diode Q-factor is determined by the formula $Q_{V1.HF}(\omega) \approx \dfrac{1}{\omega C_T r_S}$ and decreases when frequency increases. To increase the varicap diode Q-factor at high frequencies, the resistance r_S must be reduced, i.e. the thickness of n-region in the base is to be reduced. Taking into account all above-mentioned, we may conclude that the frequency dependence of the varicap diode Q-factor has a maximum with the following coordinates:

$$\frac{d\,Q_{V1}(\omega)}{d\,\omega} = \frac{C_T R_P^2 \left(R_P + r_S - \omega^2 C_T^2 R_P^2 r_S\right)}{\left(R_P + r_S + \omega^2 C_T^2 R_P^2 r_S\right)^2}; \tag{6}$$

$$\frac{d\,Q_{V1}(\omega)}{d\,\omega} = 0 \quad \Rightarrow \quad \omega_{extr} = \frac{\sqrt{1 + \dfrac{R_P}{r_S}}}{C_T R_P}; \tag{7}$$

$$Q_{V1.\max} = Q_{V1}(\omega_{extr}) = \frac{R_P}{2\sqrt{r_S\left(R_P + r_S\right)}}. \tag{8}$$

For the varicap diodes the condition $R_P >> r_S$ is satisfied (Table 1), so formulas (4) and (8) are simplified:

$$Q_{V1}(\omega) \cong \frac{\omega C_T R_P}{1 + \omega^2 C_T^2 R_P r_S}; \tag{9}$$

$$\omega_{extr} \cong \frac{1}{C_T \sqrt{R_P r_S}}; \tag{10}$$

$$Q_{V1.\max} = Q_{V1}(\omega_{extr}) \cong 0.5\sqrt{\frac{R_P}{r_S}}. \tag{11}$$

Allowing for obtained analytical relationships (7) and (8), frequency theoretical dependences of varicap diode Q-factors were constructed (solid lines in Figure 6), and coordinates of the extremum of these dependences were calculated for varicap diodes of BB149, BB174, and BB181 types manufactured by NXP Semiconductors [20–22]:

- the BB149 type varicap diode ($r_S = 0.75\,\Omega$, $R_P = 6.75\,k\Omega$, $C_T = 13\,pF$): $f_{extr} = 172.153\,MHz$; $Q_{V1.\max} = 47.434$;
- the BB174 type varicap diode ($r_S = 0.6\,\Omega$, $R_P = 6.21\,k\Omega$, $C_T = 9\,pF$): $f_{extr} = 289.852\,MHz$; $Q_{V1.\max} = 50.867$;
- the BB181 type varicap diode ($r_S = 3\,\Omega$, $R_P = 7.08\,k\Omega$, $C_T = 9\,pF$): $f_{extr} = 121.401\,MHz$; $Q_{V1.\max} = 24.29$.

The results calculated by formulas (10) and (11) differ from those calculated by formulas (7) and (8) by less than 0.1%.

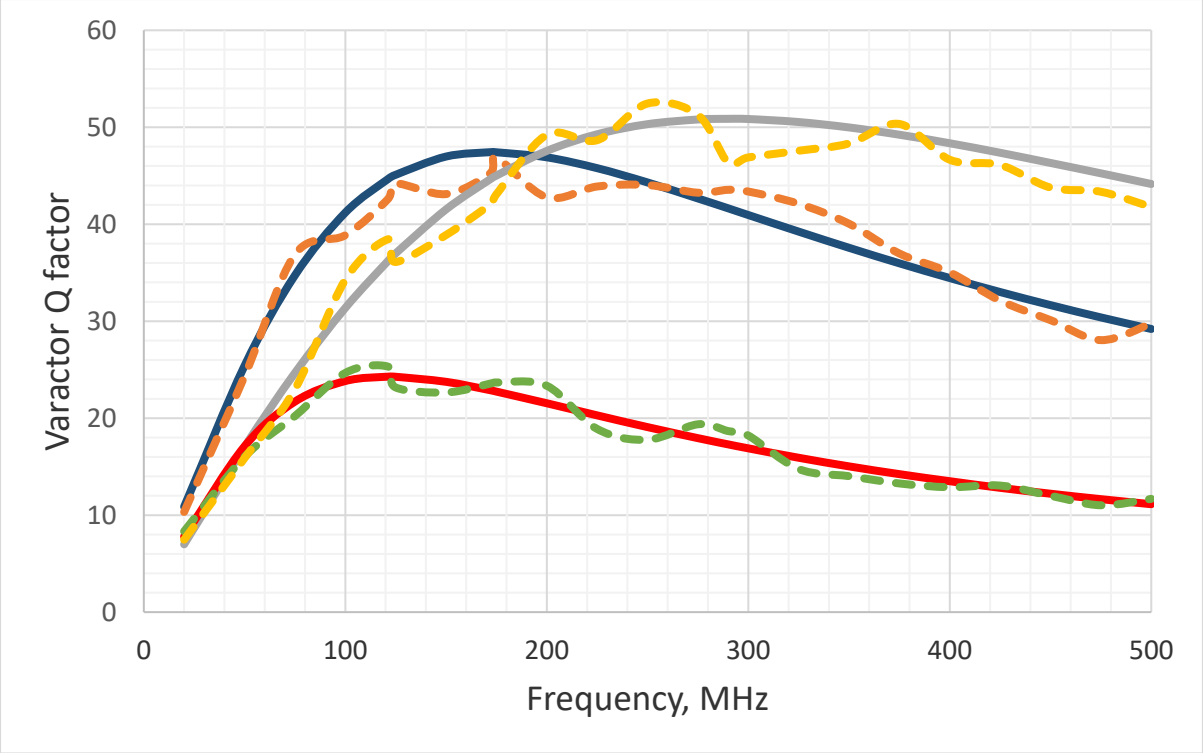

Figure 6: Theoretical (solid lines) and experimental (dashed lines) dependencies $Q_V = f(\omega)$ for the varicap diodes BB149 (blue and brown), BB174 (grey and yellow) and BB181 (red and green)

A test installation is shown in Figure 7.

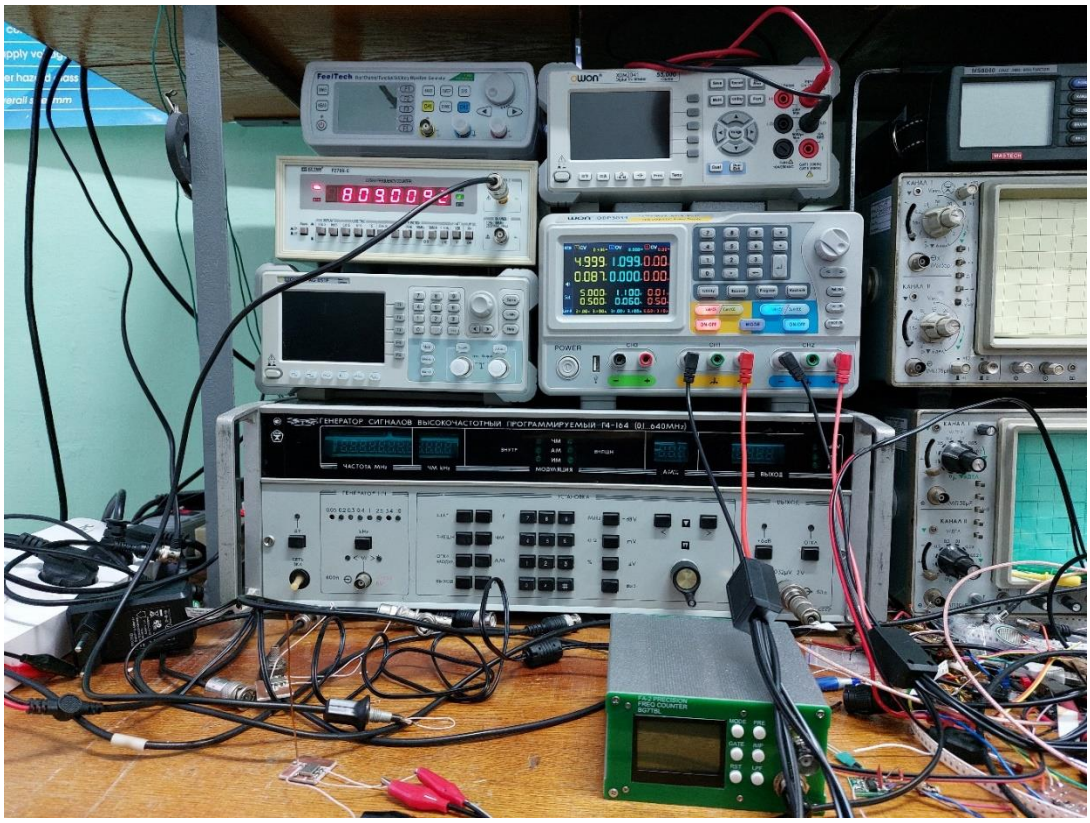

Figure 7: A test installation

Figure 6 illustrates experimental dependencies $Q_V = f(\omega)$ for the varicap diodes of BB149 (brown), BB174 (yellow) and BB181 (green) types with dotted lines. As can be seen, these experimental dependences represent theoretical ones quite accurately with a relative error no more than 8.6%. For the experimental dependences, the extremum coordinates are:

- varicap diode of BB149 type: $f_{extr} \cong 171.421\,MHz$; $Q_{V1.\max} \cong 46.883$;
- varicap diode of BB174 type: $f_{extr} \cong 260.734\,MHz$; $Q_{V1.\max} \cong 52.446$;
- varicap diode of BB181 type: $f_{extr} \cong 118.337\,MHz$; $Q_{V1.\max} \cong 25.323$.

When the temperature increases, the varicap diode Q-factor decreases due to increase in the resistance r_S. As the reverse bias increases, the capacitance C_T and resistance r_S decrease, and the Q-factor increases accordingly. The decrease of r_S when the reverse bias increases can be explained by expansion of the junction and decrease in the base thickness in n-region of the varicap diode structure [25].

The authors estimated the minimum voltage amplitude of the varicap diode in large-signal mode by linear section lengths of the Capacitance vs Reverse Voltage characteristic [20–22], which was about (2–3) V for all types of considered varicap diodes. The measurements were carried out in small-signal mode at a 0.5 V voltage across the varicap diode, (1-15) mA currents and (1~10) mW power.

4. Parameters of series and parallel equivalent circuits of the varicap diode

A varicap diode can be represented by series (Figure 8,a) or parallel (Figure 8,b) equivalent circuits [17, 26] with their parameters being determined by following relationships:

(a) (b)

Figure 8: Equivalent circuits of the varicap diode: (a) Series; (b) Parallel.

- the series equivalent circuit:

$$R_{V.series}(\omega) = \frac{R_P + r_S + \omega^2 C_T^2 R_P^2 r_S}{1 + \omega^2 C_T^2 R_P^2} \cong \frac{R_P\left(1 + \omega^2 C_T^2 R_P r_S\right)}{1 + \omega^2 C_T^2 R_P^2}, \tag{12}$$

$$C_{V.series}(\omega) = \frac{1 + \omega^2 C_T^2 R_P^2}{\omega^2 C_T R_P^2}, \tag{13}$$

$$X_{V.series}(\omega) = \frac{\omega C_T R_P^2}{1 + \omega^2 C_T^2 R_P^2}, \tag{14}$$

$$Z_V(i\omega) = R_{V.serial}(\omega) - iX_{V.serial}(\omega) = \frac{R_P\left(1 + \omega^2 C_T^2 R_P r_S\right) - i\omega C_T R_P^2}{1 + \omega^2 C_T^2 R_P^2}; \tag{15}$$

- the parallel equivalent circuit:

$$R_{V.parallel}(\omega) = \frac{\left(R_P + r_S\right)^2 + \omega^2 C_T^2 R_P^2 r_S^2}{\omega^2 C_T^2 R_P^2 r_S + R_P + r_S} \cong \frac{R_P\left(1 + \omega^2 C_T^2 r_S^2\right)}{1 + \omega^2 C_T^2 R_P r_S}, \tag{16}$$

$$C_{V.parallel}(\omega) = \frac{C_T R_P^2}{\omega^2 C_T^2 R_P^2 r_S^2 + \left(R_P + r_S\right)^2} \cong \frac{C_T}{1 + \omega^2 C_T^2 r_S^2}, \tag{17}$$

$$X_{V.parallel}(\omega)=\frac{\omega^2 C_T^2 R_P^2 r_S^2+\left(R_P+r_S\right)^2}{\omega C_T R_P^2}\cong\frac{1+\omega^2 C_T^2 r_S^2}{\omega C_T}, \tag{18}$$

$$Z_B(i\omega)=\frac{-i\,R_{V.parallel}(\omega)\,X_{V.parallel}(\omega)}{R_{V.parallel}(\omega)-i\,X_{V.parallel}(\omega)}=\frac{R_P\left(1+\omega^2 C_T^2 r_S^2\right)}{1+\omega^2 C_T^2 R_P r_S+i\omega C_T R_P}. \tag{19}$$

Figure 9 demonstrates frequency dependencies of series and parallel equivalent circuit parameters for varicap diodes BB149 ($C_T=13\,pF$), BB174 ($C_T=9\,pF$) and BB181 ($C_T=8\,pF$) types considering relationships (12), (13), (16), (17).

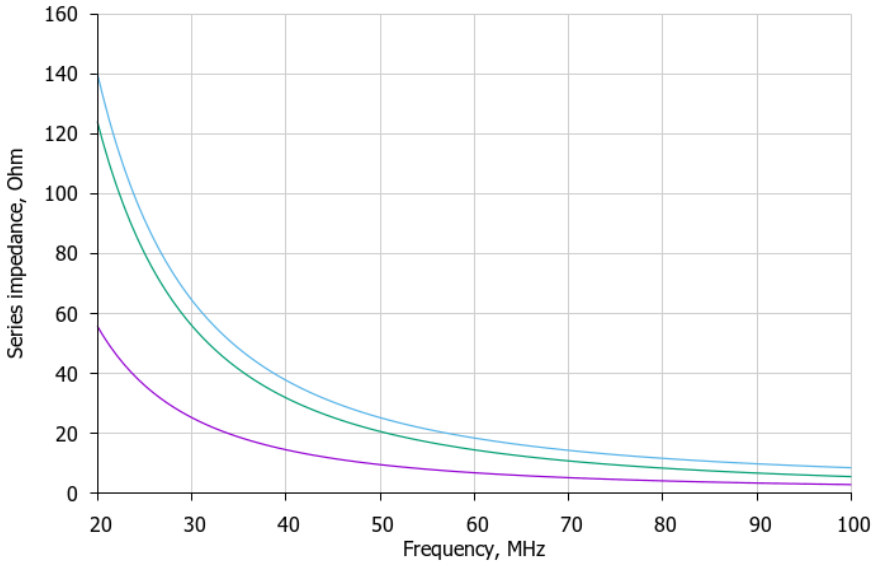

(a)

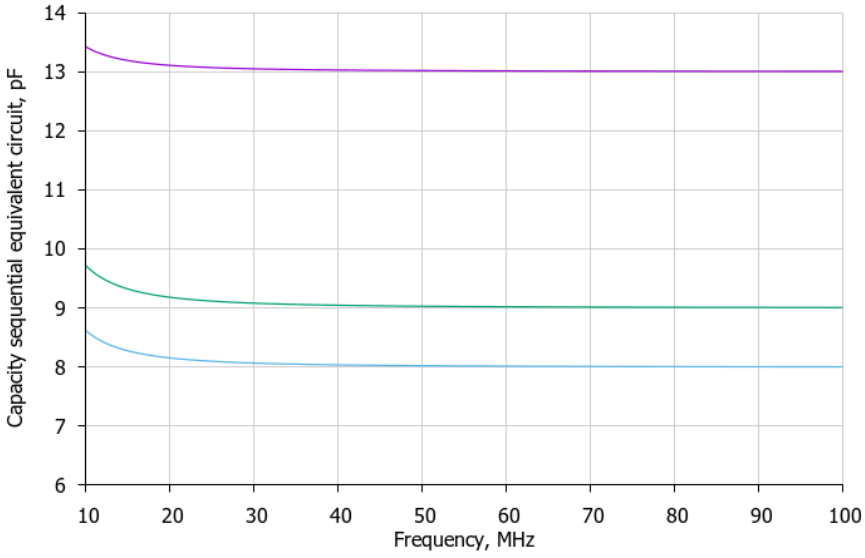

(b)

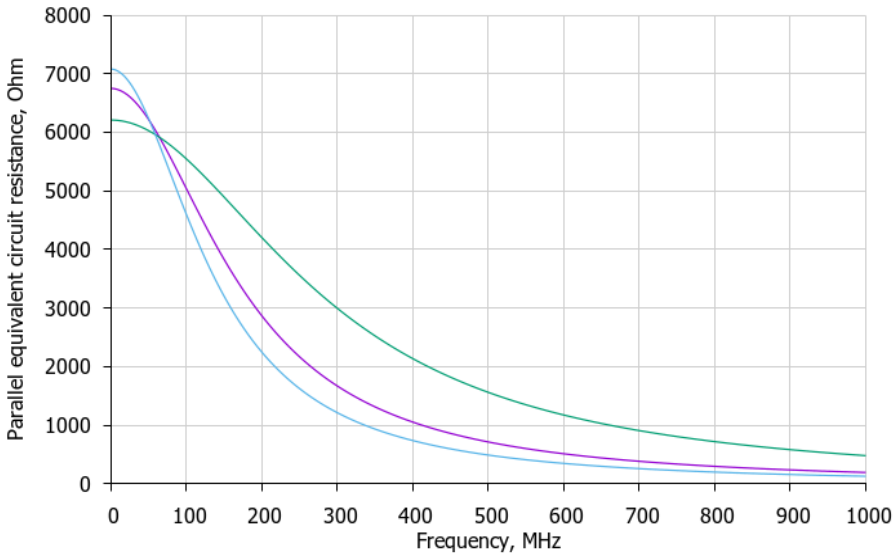

(c)

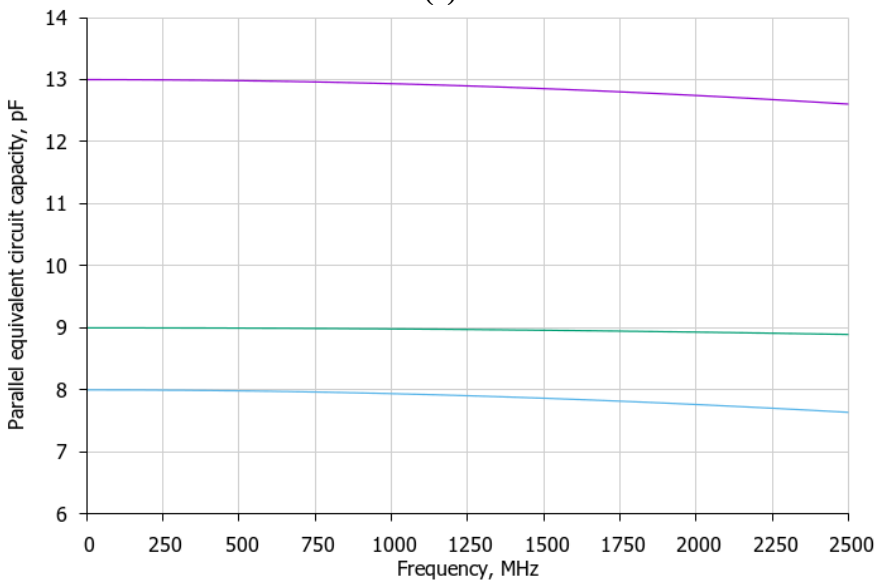

(d)

Figure 9: Frequency dependencies of equivalent circuit parameters for BB149 (purple), BB174 (green) and BB181 (blue) varicap diodes: (a) resistance of the series equivalent circuit (Ohm); (b) capacity of the series equivalent circuit (pF); (c) resistance of the parallel equivalent circuit (Ohm); (d) capacity of the parallel equivalent circuit (pF)

From the dependencies shown in Figure 9 we may made the following conclusions:

- the dependencies $R_{V.series}(f)$ and $R_{V.parallel}(f)$ verge to the value $R_P + r_S \cong R_P$ at low frequencies and to r_S at high frequencies (Figures 9,a,c);
- the dependence $C_{V.series}(f)$ verges to infinity at low frequencies and to the value C_T at high frequencies (Figure 9,b);
- the dependence $C_{V.parallel}(f)$ is almost equal to the value C_T at low frequencies and verges to zero at high frequencies (Figure 9,d).

The frequency f_1, at which the capacity $C_{V.series}$ differs from the capacity C_T by less than 0.5%, is:

$$\frac{1+\omega_1^2 C_T^2 R_P^2}{\omega_1^2 C_T R_p^2} = 1.005\, C_T \quad \Rightarrow \quad f_1 = \frac{7.071}{\pi C_T R_P} \cong \frac{2.252}{C_T R_P}. \tag{20}$$

For the BB149 type varicap diode at $C_T = 13\ pF$ the frequency f_1 equals 25.66 MHz, for the BB174 type varicap diode at $C_T = 9\ pF$ it is equal to 40.29 MHz and for the BB181 type varicap diode at $C_T = 8\ pF$ it is 39.76 MHz.

The frequency f_2, at which the active resistance $R_{V.series}$ differs from the resistance r_S by less than 3%, is:

$$\frac{R_P + r_S + \omega_2^2 C_T^2 R_P^2 r_S}{1 + \omega_2^2 C_T^2 R_P^2} = 1.03\, r_S \quad \Rightarrow \quad f_2 = \frac{2.887}{\pi C_T \sqrt{R_P r_S}} \cong \frac{0.919}{C_T \sqrt{R_P r_S}}. \tag{21}$$

For the BB149 type varicap diode at $C_T = 13\ pF$ the frequency f_2 equals 993.5 MHz, for the BB174 type varicap diode at $C_T = 9\ pF$ it is equal to 1672.8 MHz and for the BB181 type varicap diode at $C_T = 8\ pF$ it is 788.2 MHz.

The frequency f_3, at which the capacity $C_{V.parallel}$ differs from the capacity C_T by less than 0.5%, is

$$\frac{C_T R_P^2}{\omega_3^2 C_T^2 R_P^2 r_S^2 + \left(R_P + r_S\right)^2} = 0.99 C_T \quad \Rightarrow \quad f_3 = \frac{1}{2\pi\sqrt{199}\, C_T r_S} \cong \frac{0.0113}{C_T r_S}. \tag{22}$$

For the BB149 type varicap diode at $C_T = 13\ pF$ the frequency f_3 equals 1159 MHz, for the BB174 type varicap diode at $C_T = 9\ pF$ it is equal to 2093 MHz and for the BB181 type varicap diode at $C_T = 8\ pF$ it is 470.8 MHz.

The frequency f_4, at which the active resistance $R_{V.parallel}$ differs from the resistance r_S by less than 3%, is:

$$\frac{\left(R_P + r_S\right)^2 + \omega_4^2 C_T^2 R_P^2 r_S^2}{\omega_4^2 C_T^2 R_P^2 r_S + R_P + r_S} = 1.03 r_S \quad \Rightarrow \quad f_4 = \frac{1}{2\pi\sqrt{0.03}\, C_T r_S} \cong \frac{0.919}{C_T r_S}. \tag{23}$$

For the varicap diode of BB149 type at $C_T = 13\ pF$ the frequency f_4 equals 94.256 GHz, for the varicap diode of BB174 type at $C_T = 9\ pF$ it is equal to 170.185 GHz and for the varicap diode of BB181 type at $C_T = 8\ pF$ it is 38.292 GHz.

If the varicap diode frequency range is limited by the range $Q_V \geq Q_{V0}$, we obtain:

$$f_{\min} = \frac{Q_{V0}}{2\pi C_T R_P}, \tag{24}$$

$$f_{\max} = \frac{1}{2\pi Q_{V0} C_T r_S}. \tag{25}$$

For the BB149 type varicap diode for $Q_V \geq 35$ this frequency range $\left[f_{\min} \div f_{\max}\right]$ corresponds to $\left(63.51 \div 466.62\right)$ MHz, for the BB174 type varicap diode for $Q_V \geq 35$ it corresponds to $\left(99.72 \div 842.52\right)$ MHz and for the BB181 type varicap diode for $Q_V \geq 15$ it corresponds to $\left(42.17 \div 442.32\right)$ MHz.

The Q-factors of 35 and 15 were chosen considering the frequency characteristics (Figure 6) about the passband level, that is a 0.707 level from the maximum value of the varicap diode Q-factor.

The capacitance of varicap diodes of BB149, BB174 and BB181 types in any equivalent circuit diverges from the varicap diode junction equivalent capacitance in these frequency ranges by no more than 0.5%. Therefore, we can assume that $C_{V.series}(\omega) \cong C_{V.parallel}(\omega) \cong C_T$. Eventually, for the BB149 type varicap diode in the $\left(25.66 \div 1159\right)$ MHz frequency range, for the BB174 type varicap diode in the $\left(40.29 \div 2093\right)$ MHz frequency range and for the BB181 type varicap diode in the $\left(39.76 \div 470.8\right)$ MHz frequency range the next formulas can be written with an error less than 0.5%:

$$Z_{V.series}(i\omega) \cong \frac{R_P\left(1+\omega^2 C_T^2 R_P r_S\right)}{1+\omega^2 C_T^2 R_P^2} - i\frac{1}{\omega C_T}, \tag{26}$$

$$Z_{V.parallel}(i\omega) \cong \frac{R_P\left(1+\omega^2 C_T^2 r_S^2\right)}{1+\omega^2 C_T^2 R_P r_S + i\omega C_T R_P\left(1+\omega^2 C_T^2 r_S^2\right)}, \tag{27}$$

$$Q_{V.series}(i\omega) = Q_{V.parallel}(i\omega) \cong \frac{1+\omega^2 C_T^2 R_P^2}{\omega C_T R_P\left(1+\omega^2 C_T^2 R_P r_S\right)}, \tag{28}$$

that is, the varicap diode in the equivalent circuit can be superseded by a series or parallel connection of a resistor with resistance being a function of frequency, and a capacitor with capacitance being independent of frequency and determined by the equivalent varicap diode junction capacitance [17].

For both serial and parallel equivalent circuits of the varicap diode, its quality factor is determined by formula (28).

If the noise is present in the measuring instrument channels, then a random component of uncertainty arises; the authors propose to estimate it by the next formula [18]:

$$s_N = \sqrt{\frac{q_1 + q_2 + \sqrt{q_1 q_2}\sin\varphi}{q_1 q_2}}, \tag{29}$$

where $q_1 = \frac{P_1}{s_1^2}$ and $q_2 = \frac{P_2}{s_2^2}$ are the signal-to-noise ratio in the measuring instrument channels; s_i is the root-mean-square values of noise in the measuring instrument channels; P_i is a power of signal; φ is a phase shift proportional to the time delay of a signal in the channel.

The Allan variance method was proposed in [27] to be applied for identifying the noise structure in the measuring instrument channels.

5. Conclusion

In the paper the authors showed that the varicap diode Q-factor is determined by parameters of the small-signal equivalent circuit and is a function of frequency. We analyzed the effect of barrier capacitance, junction resistance, and loss resistance of the varicap diode on its Q-factor in low and high frequency ranges. We obtained formulas that provide determining the maximum value of the varicap diode Q-factor and the frequency corresponding to its maximum Q-factor. We experimentally tested theoretical results for three different varicap diodes of BB149, BB174 and BB181 types manufactured by NXP Semiconductors. Deviations of the theoretical results from experimental testing in the (20 ÷ 500) MHz frequency range were less than 8.6%. We established that the frequency range in which the Q-factor $Q_V \geq 35$ for varicap diodes of BB149 and BB174 types was $(63.51 \div 466.62)$ MHz and $(99.72 \div 842.52)$ MHz, and for the BB181 type varicap diode at $Q_V \geq 15$ it was $(42.17 \div 442.32)$ MHz.

We obtained formulas that determine active and reactive parameters of the elements in the series and parallel equivalent circuits of the varicap diode. We analyzed frequency dependences of the varicap diode Q-quality factor and parameters of the series and parallel equivalent circuits. This promoted to simplify the formulas for determining parameters of the elements in the series and parallel equivalent circuits in the operating frequency range, where the varicap diode Q-factor is more than $0.707Q_{V.\max}$. We proved that in the frequency ranges of $(25.66 \div 1159)$ MHz for the BB149 varicap diode, $(40.29 \div 2093)$ MHz for the BB174 varicap diode, and MHz for the $(39.76 \div 470.8)$ BB181 varicap diode, equivalent capacitances of the series and parallel equivalent circuits differed from the junction barrier capacitance by less than 0.5%. Therefore, in the specified frequency ranges, the varicap diode in the equivalent circuit can be replaced by a series or parallel connection of a resistor, whose resistance is a function of frequency and is determined by formulas (12) or (16), and a capacitor, whose

capacitance does not depend on frequency and is determined by the equivalent capacitance of the varicap diode junction.

Theoretical assumptions and simulation results are confirmed by the experimental testing results. The authors proposed a method for estimating the maximum frequency of the operating frequency range of a varicap diode using SPICE Model Parameters, provided that the reactive capacitance of the varicap diode is an order of magnitude greater than the inductive resistance of its leads.

The practical application of the study is that the authors had obtained formulas for determining the frequency spectrum with the Q-factor higher than a given value.

Further development of the study is evaluating the influence of the varicap diode characteristic nonlinearity in the of a large-signal mode with more than 2 V amplitude, various types of noise and temperature instabilities on the frequency dependence of the varicap diode Q-factor.

6. Acknowledgements

This work was supported by the Ministry of Education and Science of Ukraine, grant No. 0121U109722 “Methods and devices for forming and processing chaotic signals, access control and positioning in robotic and infocommunication systems”.

7. References

[1] G. Maget, Varactors and Inductors for Integrated RF Circuits in Standard MOS Technologies, Dr.-Eng. thesis, Universität der Bundeswehr München, Neubiberg, Germany, 2002.

[2] A. S. Nagra, Varactor loaded transmission lines for linear applications, Ph.D. Comprehensive Exam Presentation, University of California at Santa Barbara, Santa Barbara, CA, USA, 1999.

[3] D. Lee, A. Nikoofard, P.P. Mercier, A −254.1-dB FoM 2.4-GHz Subsampling PLL With a −76-dBc Reference Spur by Employing a Varactor-Based Cancellation Technique, IEEE Solid-State Circuits Letters 3 (2020) 102-105. doi:10.1109/LSSC.2020.3007687.

[4] W. Deng, D. Yang, T. Ueno, T. Siriburanon, S. Kondo, K. Okada, A. Matsuzawa, A Fully Synthesizable All-Digital PLL With Interpolative Phase Coupled Oscillator, Current-Output DAC, and Fine-Resolution Digital Varactor Using Gated Edge Injection Technique, IEEE Journal of Solid-State Circuits 50 (2015) 68-80. doi:10.1109/JSSC.2014.2348311.

[5] L. M. Dani, N. Mishra, A. Bulusu, An Efficient and Accurate Variation-Aware Design Methodology for Near-Threshold MOS-Varactor-Based VCO Architectures, IEEE Transactions on Computer-Aided Design of Integrated Circuits and Systems 40 (2021) 2117-2127. doi:10.1109/TCAD.2020.3037881.

[6] X. Gui, B. Tang, R. Tang, D. Li, L. Geng, Low-Supply Sensitivity LC VCOs With Complementary Varactors, IEEE Transactions on Very Large Scale Integration (VLSI) Systems 28 (2020) 1589-1599. doi:10.1109/TVLSI.2020.2991765.

[7] Y. Kim, S. Hong, A W-Band Vector Modulator Using Short-Channel Transistor Current Sources and Impedance Compensation Varactors, IEEE Transactions on Circuits and Systems II: Express Briefs (2022). doi:10.1109/TCSII.2022.3171448.

[8] D. Vovchuk, S. Haliuk, P. Robulets, Development of Frequency Modulator with SplitRing Resonator Loaded by Varactor Diode, in: Proceedings of the 2020 IEEE 15th International Conference on Advanced Trends in Radioelectronics, Telecommunications and Computer Engineering, TCSET, 2020, pp. 536-539. doi:10.1109/TCSET49122.2020.235490.

[9] R. Fiorelli, M. Delgado-Restituto, Á. Rodríguez-Vázquez, Offset-Calibration With Time-Domain Comparators Using Inversion-Mode Varactors, IEEE Transactions on Circuits and Systems II: Express Briefs 67 (2020) 47-51. doi:10.1109/TCSII.2019.2904100.

[10] M. Zlochisti, Seyed Alireza Zahrai, M. Onabajo, Digitally programmable offset compensation of comparators in flash ADCs for hybrid ADC architectures, in: Proceedings of the 2015 IEEE 58th International Midwest Symposium on Circuits and Systems, MWSCAS, 2015, pp. 1-4. doi:10.1109/MWSCAS.2015.7282059.

[11] A. Singh, M. K. Mandal, Electronically Tunable Reflection Type Phase Shifters, IEEE Transactions on Circuits and Systems II: Express Briefs 67 (2020) 425-429. doi:10.1109/TCSII.2019.2921036.
[12] A.J. Antony, A.A. Sudesh, A. Mohamed, R. Gopika, A. Mitra, D. Sarkar, C. Saha, Design of a 360° Continuously Variable Phase Shifter using Improved Regression Algorithm for X-band Phased Array Applications, in: Proceedings of the 2021 IEEE MTT-S International Microwave and RF Conference, IMARC, 2021, pp. 1-4. doi:10.1109/IMaRC49196.2021.9714640.
[13] R. H. Kenney, C. J. Walker, H. H. Sigmarsson, J. W. McDaniel, A Varactor-Based Tunable Combline Bandpass Filter Using Suspended Integrated Stripline (SISL), IEEE Journal on Miniaturization for Air and Space Systems 2 (2021) 112-116. doi:10.1109/JMASS.2020.3029581.
[14] P.Ö. Özdemir, A. Öztürk, A.K. Görür, C. Karpuz, A. Görür, An Alternative Application to Tune the Center Frequency of a Microstrip Balun Bandpass Filter, in: Proceedings of the 2019 European Microwave Conference in Central Europe, EuMCE, 2019, pp. 162-165.
[15] S. Li, S. Chen, J. Cai, X. Zhou, G. Wang, T. Liu, A Bandwidth Enhanced Outphasing Power Amplifier, in: Proceedings of the 2021 Cross Strait Radio Science and Wireless Technology Conference, CSRSWTC, 2021, pp. 160-162. doi:10.1109/CSRSWTC52801.2021.9631561.
[16] Z. Wang, D. Hou, P. Zhou, H. Li, Z. Li, J. Chen, W. Hong, A Ka-Band Switchable LNA With 2.4-dB NF Employing a Varactor-Based Tunable Network, IEEE Microwave and Wireless Components Letters 31 (2021) 385-388. doi:10.1109/LMWC.2021.3059655.
[17] A.V. Rudyk, A.O. Semenov, N. Kryvinska, O.O. Semenova, Measuring quality factors of the radio-frequency system components using equivalent circuits, Journal of Computational Electronics 20 (2021) 1977-1991. doi:10.1007/s10825-021-01770-z.
[18] A. Rudyk, A. Semenov, N. Kryvinska, O. Semenova, Study of phase and amplitude-phase methods for measuring a reactive element quality factor, Measurement 187 (2022) 110271. 10.1016/j.measurement.2021.110271.
[19] D.R. Chase, Lee-Yin Chen, and R.A. York, Modeling the capacitive nonlinearity in thin-film BST varactors, IEEE Transactions on Microwave Theory and Techniques 53 (2005) 3215-3220. doi:10.1109/TMTT.2005.855141.
[20] BB149, UHF variable capacitance diode, Product data sheet, 2011. URL: https://www.nxp.com/docs/en/data-sheet/BB149.pdf
[21] BB174, VHF variable capacitance diode, Product data sheet, 2013. URL: https://www.nxp.com/docs/en/data-sheet/BB174.pdf
[22] BB181, VHF variable capacitance diode, Product data sheet, 2009. URL: https://www.nxp.com/docs/en/data-sheet/BB181.pdf
[23] T.S. Price, Nonlinear Properties of Nanoscale Barium Strontium Titanate Microwave Varactors, Ph.D. thesis, University of South Florida, Tampa, Fl, USA, 2012.
[24] A. Semenov, S. Baraban, M. Baraban, O. Zhahlovska, S. Tsyrulnyk, A. Rudyk, Development and Research of Models and Processes of Formation in Silicon Plates p-n Junctions and Hidden Layers under the Influence of Ultrasonic Vibrations and Mechanical Stresses, Key Engineering Materials 844 (2020) 155–167. doi:10.4028/www.scientific.net/kem.844.155.
[25] R. Amirpour, D. Schwantuschke, P. Brueckner, R. Quay, O. Ambacher, High-Q Anti-Series AlGaN/GaN High Electron-Mobility Varactor, in: Proceedings of the 2019 IEEE MTT-S International Microwave Symposium, IMS, Boston, MA, USA, 2019, pp. 599-602. doi:10.1109/MWSYM.2019.8700797.
[26] A.O. Semenov, O.M. Voznyak, O.V. Osadchuk, S.V. Baraban, O.O. Semenova, A.V. Rudyk, J. Klimek, S. Orazalieva, Development of a non-standard system of microwave quadripoles parameters, Proceedings of SPIE 11176 (2019) 111765N. doi:10.1117/12.2536704.
[27] A. V. Rudyk, A. O. Semenov, N. Kryvinska, O. O. Semenova, V. P. Kvasnikov, A. P. Safonyk, Strapdown Inertial Navigation Systems for Positioning Mobile Robots – MEMS Gyroscopes Random Errors Analysis Using Allan Variance Method, Sensors 20 (2020) 4841. doi:10.3390/s20174841.